Acta Geod Geophys (2016) 51:671–683
DOI 10.1007/s40328-015-0146-0

An application of AVO derived attributes to analyze seismic anomalies of gas hydrate bearing sediments in Makran offshore, Pakistan

Muhammad Irfan Ehsan[1] · Nisar Ahmed[2] · Zia Ud Din[2] · Perveiz Khalid[2] · Liu Xue Wei[1]

Received: 12 March 2015 / Accepted: 17 October 2015 / Published online: 28 October 2015

Abstract The presence of gas hydrates in Makran area of Pakistan is confirmed by seismic evidences in the form of a strong reflector known as bottom simulating reflector (BSR). Amplitude versus offset (AVO) analysis is performed to analyze seismic behavior of free gas zone beneath BSR. This analysis is carried by considering a free gas zone beneath a gas hydrate-bearing zone and overlying a fully water saturated interval. Different pairs of AVO-derived attributes are applied to differentiate free gas and gas hydrates saturated sediments. Based on our analysis, it is concluded that low and high saturation of gas hydrates can be deduced from seismic amplitude anomalies. Low and high saturation of gas hydrates can be distinguish able from background trend. The fluid factor, pore space modulus and Poisson reflectivity are found more sensitive attributes for discrimination of gas hydrates saturation.

Keywords Makran offshore · Seismic attributes · Gas hydrates · Fluid indicator coefficients

1 Introduction

Gas hydrates are clathrate composed of water and natural gas formed under low temperature and high pressure conditions (Kvenvolden 1998; Sloan 1998). Gas hydrate molecule, contains low molecular hydrocarbon gases such as methane (CH_4), and higher molecular hydrocarbon chains like ethane (C_2H_6), propane (C_3H_8) and butane (C_4H_{10}) in small concentration, is trapped in the cage of water molecules (Hardage and Roberts 2006). Gas

✉ Muhammad Irfan Ehsan
irfan_opq@yahoo.com

[1] School of Geophysics and Information Technology, China University of Geosciences, Beijing 100083, China

[2] Institute of Geology, University of the Punjab, Lahore 54590, Pakistan

hydrates have taken large attraction because of their wide distribution in permafrost and their large potential as unconventional energy resource for future (Dillon et al. 1991; Paull et al. 1991; Taylor and Kwan 2004; Makogon et al. 2007). Bottom simulating reflector

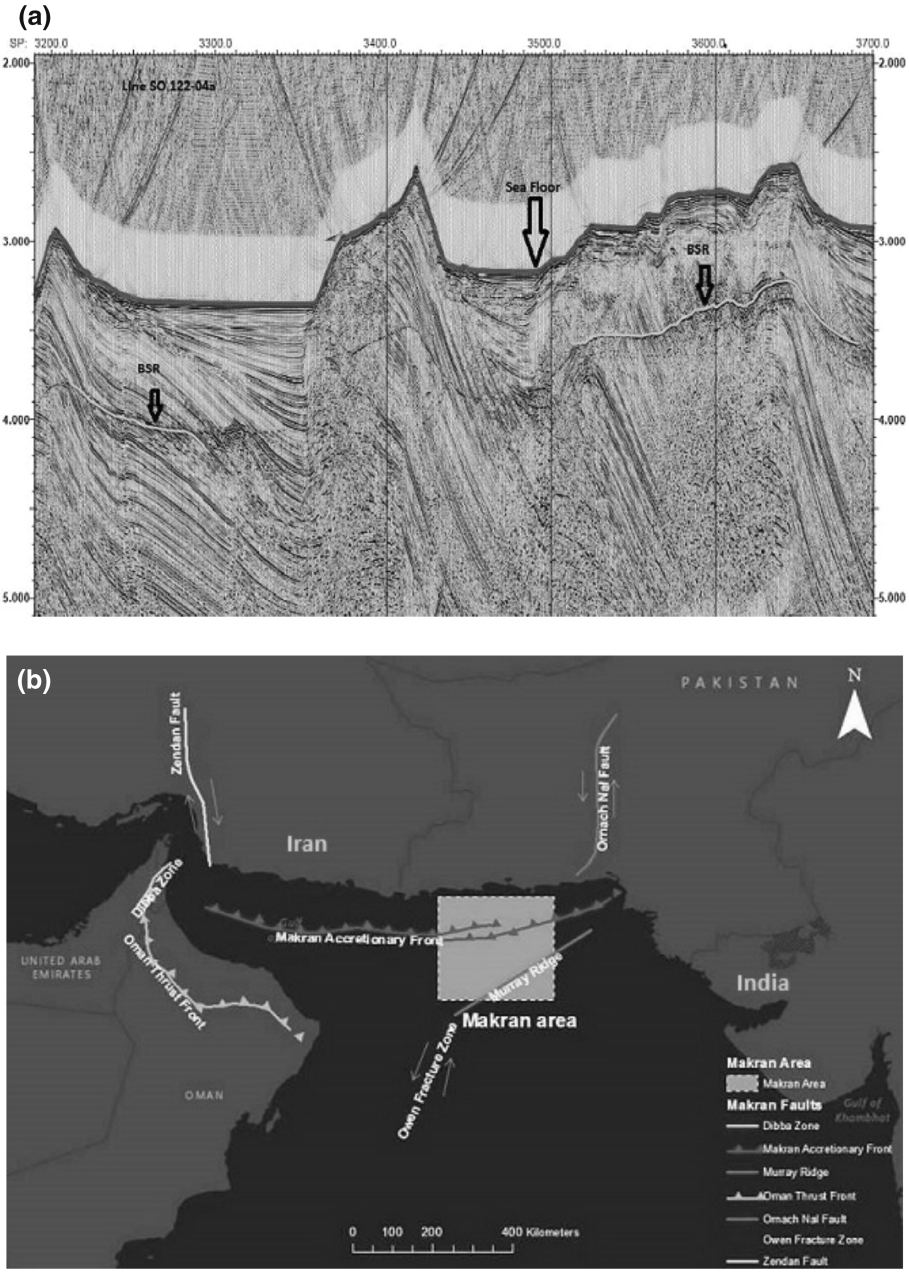

Fig. 1 **a** Seismic section from Makran area of Pakistan showing strong bottom simulating reflector (BSR) represents to the presence of gas hydrates (Ehsan et al. 2015) and **b** location map of Makran area of Pakistan

(BSR) on seismic section is interpreted as seismic detector for the presence of gas hydrates bearing formation (Fig. 1a). A free gas zone in general present just below the BSR (Anderson et al. 1990).

We generally identify BSR based on some prominent characteristics, (i) containing large amplitude by showing opposite polarity with respect to the sea floor reflection, (ii) cutting across the dipping sedimentary strata and (iii) mimicking sea floor topography (Sain and Gupta 2012). However, the quantitative estimation of gas hydrates and free gas beneath gas hydrate-bearing sediments is not easy. In some areas, where no direct observations available for quantitative analysis of seismic signatures appear from gas hydrate-bearing sediments and free gas beneath gas hydrate-bearing layer, amplitude versus offset (AVO) analysis or seismic attributes can be used (Ojha and Sain 2008; Ojha et al. 2010). In seismic data interpretation, AVO attributes have taken reasonable attention to sort out desired lithology and reservoir estimation (Castagna and Backus 1993; Castagna and Smith 1994; Castagna et al. 1998). Since, in Makran area (Fig. 1b), no direct measurements are available to quantify the concentration of gas hydrates and free gas beneath the gas hydrate-bearing sediments, therefore AVO analysis is very useful technique for quantitative estimation of gas hydrates concentration and free gas distribution into the pore spaces (Hyndman and Spence 1992; Andreassen et al. 1997; Ecker et al. 1998; Yuan et al. 1999; Carcione and Tinivella 2000; Chen et al. 2007).

In previous work (Ehsan et al. 2015) AVO analysis was performed to see the effect of gas hydrates saturation on seismic amplitudes and the effect of gas hydrates saturation was clearly demonstrated on the seismic amplitudes. In this work, various AVO-derived attributes are studied to find the best attribute which can quantify gas hydrate saturation from brine saturated porous rock. For computation of intercept I, gradient G, Poisson reflectivity PR, fluid factor, etc. we have used effective medium theory (Khalid et al. 2014) and Gassmann fluid substitution approach (1951). Theoretical mapping of gas hydrate reservoir for different AVO derived attributes provide an intuitive approach to identify BSR and quantify weather BSR is related gas hydrate bearing sediments (Ojha and Sain 2009; Ojha et al. 2010).

2 Geology and stratigraphy

South western part of Pakistan has prominent geo tectonic arrangements where Eurasian, Arabian and Indian plates are intersecting each other. Gulf Oman offshore in the west is subducting northward beneath the Afghan plate (Farhoudi and Karig 1977). Makran area represents EW enhancing prism which formed with continuity of subduction since craterous. A wedge has been developed between buried trench and its larger segment overlying Arabian plate showing dipping trend at shallow angle (White 1979; Quittmeyer et al. 1979). Stratigraphic record gives a fruitful clue that evolution of Makran arc trench takes place in Cenozoic era (Stoneley 1974). Stratigraphy of the Makran offshore is established on the basis of northern outcrops of coastal line. Panjgur Formation of Upper Oligocene–Lower Miocene age is the oldest rock exposed in this area. Other formations reported in this area are Parkini Shale of Upper Miocene, Talar Formation of Lower Pliocene, Chatti and Ormara Formations of Pleistocene and Jiwani Formation of Holocene age. Towards Makran offshore, these sediments become younger and underlain by the mud/mudstone (Harms et al. 1982).

3 Methodology

In the present section, we have described a complete quantitative work flow used to perform fluid substitution modeling (FSM) and to extract the AVO attributes for gas hydrate bearing sediments in Makran area. Different input parameters are derived by using modified effective medium theory (Ehsan et al. 2015). FSM is a fundamental step in AVO analysis (Russell et al. 2003; Khalid et al. 2014; Ahmed et al. 2015), which leads us to interpret the gas hydrate reservoirs quantitatively. In first step, we have performed Gassmann's (1951) FSM by using available petrophysical parameters for gas hydrate-bearing sediments in the Makran area of Pakistan. Gassmann's equation is the focus point to illustrate how pore fluids type, saturation and spatial distribution patterns influence on the physical properties such as elastic moduli, seismic velocities, etc. (Hill 1963). Gassmann's equation gives mathematical relationship to compute the saturated rock bulk modulus, when the distribution within the pore fluid is in the form of patchy. The Hill's relationship for saturated bulk modulus is given below. The rock physics parameters used in this study are presented in Table 1.

$$K_{sat} = \left[\frac{S_w}{K_{satw} + 4/3\mu_{sat}} + \frac{1 - S_w}{K_{satH} + 4/3\mu_{sat}}\right]^{-1} - \frac{4}{3}\mu_{sat}, \quad (1)$$

where S_w is the saturation of water, K_{sat} is the bulk modulus of saturated sediments and K_{satw} and K_{satH} are bulk modulus of sediments when saturated with water and gas hydrates, respectively. As fluid does not produce shearing effect, so the shear modulus of dry rock is equal to the saturated shear modulus, thus

$$\mu_{sat} = \mu_{dry}. \quad (2)$$

Table 1 Parameters used in effective medium modeling when gas hydrates are part of fluids (Ehsan et al. 2015)

Parameters	Symbols	Numerical values	Units
Porosity	ϕ	39	%
Critical porosity	ϕ_c	36	%
Dry rock bulk modulus	K_{dry}	1.028	GPa
Dry rock shear modulus	G_{dry}	1.432	°GPa
Number of grains per contact	n	9	
Quartz bulk modulus	K_q	37	GPa
Quartz shear modulus	G_S	45	GPa
Clay bulk modulus	K_c	20.9	GPa
Clay shear modulus	G_c	6.85	GPa
Quartz density	ρ_q	2.65	g/cm^3
Clay density	ρ_c	2.58	g/cm^3
Gas hydrate bulk modulus	K_h	6.41	GPa
Gas hydrate shear modulus	G_h	2.54	GPa
Gas hydrate density	ρ_h	0.91	g/cm^3
Gas bulk modulus	K_g	0.067	GPa
Gas density	ρ_g	0.20	g/cm^3
Water bulk modulus	K_W	2.25	GPa
Density of water	ρ_w	1.0	g/cm^3

Seismic velocities of compressional and shear waves (α and β, respectively) can be computed by using following relation:

$$\alpha = \left(\frac{K_{sat} + \frac{4}{3}\mu_{sat}}{\rho_{eff}} \right)^{1/2}, \tag{3}$$

$$\beta = \left(\frac{\mu_{sat}}{\rho_{eff}} \right)^{1/2}. \tag{4}$$

The effective density (ρ_{eff}) of the gas hydrates bearing sediments is the function of porosity, density of solid rock (ρ_s) and density of fluid (ρ_f). It can be calculated by using following equation

$$\rho_{eff} = (1 - \phi)\rho_s + \phi\rho_f. \tag{5}$$

As P wave reflection coefficient (R_{PP}) at an interface is the function of α, β and ρ_{eff} of both upper and lower mediums. In this work the upper layer consists of gas hydrate bearing sediments and lower layer consists of free gas saturated sediments, in which seismic velocities and effective density is calculated by FSM at different saturation levels.

Now we have discussed the work flow of empirical relations used to derived the various AVO-derived attributes such as intercept (I), gradient (G), their product ($I * G$), Poisson reflectivity (PR), fluid factor (ΔF), pore space modulus (K_P), etc. and some other rock physics parameters like Lame's parameter (λ). The most common AVO attributes are intercept (normal incident reflection coefficient) and gradient (rate at which magnitude of reflection amplitude varies as a function of angle/offset). Shuey (1985) approximated the Zoeppritz (1919) mathematical relation into simplified form in term of intercept and gradient as given below:

$$R_{PP}(\theta) = I + G\sin^2\theta, \tag{6}$$

whereas

$$I = \frac{1}{2}\left(\frac{\Delta\alpha}{\alpha_{ave}} + \frac{\Delta\rho_{eff}}{\rho_{effave}} \right), \tag{7}$$

and

$$G = -2\frac{\beta_{ave}^2}{\alpha_{ave}^2}\frac{\Delta\rho_{eff}}{\rho_{effave}} + \frac{1}{2}\frac{\Delta\alpha}{\alpha_{ave}} - 4\frac{\beta_{ave}^2}{\alpha_{ave}^2}\frac{\Delta\beta_{ave}^2}{\alpha_{ave}^2}\frac{\Delta\beta}{\beta_{ave}}. \tag{8}$$

Here $\Delta\alpha$, $\Delta\beta$ and $\Delta\rho_{eff}$ represent the difference in compressional wave velocity and shear wave velocity and effective density across the gas hydrate bearing interface and α_{ave}, β_{ave}, and ρ_{effave} are average compressional and shear wave velocities and density for upper and lower medium. After computing intercept and gradient, many other attributes like their product ($I * G$), average of their difference ($I - G/2$) and sum ($I + G/2$) can be derived easily.

Interpretation of AVO anomaly for gas hydrate bearing sediments can be made by cross plotting of intercept and gradient. However, the accuracy of this method strongly depends on correct prediction of background trend. PR introduced by Verm and Hilterman (1995) is also an important AVO indicator which depends on Poisson's ratio of upper (v_1) and lower (v_2) medium and can be calculated by using a mathematical relationship given as:

$$PR = \frac{(v_2 - v_1)}{[1 - (v_1 + v_2)/2]^2}. \tag{9}$$

Fluid factor (ΔF) given by Smith and Gidlow (1987) is also a reliable indicator for BSR identification (Yang et al. 2014). The empirical relationship for fluid factor is given below:

$$\Delta F = I - 1.16\left(\frac{\beta_{ave}}{\alpha_{ave}}\right)R_s. \tag{10}$$

Here R_s is the normal incidence reflectivity for S wave. In order to sort out most reliable attribute for gas hydrate bearing sediments, we have tested different attributes and found Lame's parameter (λ) and pore space modulus (K_P) most suitable for gas hydrates discrimination. Mathematical description for Lame's parameters is given below:

$$\mu_{sat} = \beta^2 \rho_{eff}, \tag{11}$$

$$\lambda = K_{sat} - \frac{2\mu_{sat}}{3}. \tag{12}$$

The idea of pore space modulus (K_P) was given by Hedlin (2000). He has used Gassmann's poroelastic equation to build up relationship for clean sand by computing $K_{dry}/\mu = 0.9$

$$K_P = \rho_{eff}\left(\alpha^2 - 2.333\beta^2\right). \tag{13}$$

Since, gas hydrates bearing sediments contain about 13.5 % clay, therefore, the modified value of K_P by using $K_{dry}/\mu = 1.0573$ is

$$K_P = \rho_{eff}\left(\alpha^2 - 2.3906\beta^2\right). \tag{14}$$

In the present study, all the above mentioned attributes are computed at 11 different depth intervals within the gas hydrate bearing sediments by considering different saturation levels of binary phase fluids (gas hydrates/brine). Different attributes are crossplotted to visualize the discrimination of gas hydrate sediments from the brine saturated sediments.

The fluid indicator coefficient (FIC) is used to elaborate which attribute is most suitable to distinguish gas hydrate reservoir when they are part of fluid. FIC is defined as the ratio of the difference of mean value of any attribute fully saturated with water (m_b) and mean value of any attribute at certain saturation of gas hydrates (m_h) over standard deviation ($s{\cdot}t_h$). The mathematical description for (FIC) is given below (Dillon et al. 2003).

$$FIC = \frac{m_b - m_h}{s \cdot t_h}. \tag{15}$$

In above equation m represent mean value of any attribute and the subscripts b and h describe the attributes fully saturated with brine and gas hydrates which we want to compute.

4 Results

Seismic reflectivity from gas hydrate bearing sediments strongly depends on the saturation level of gas hydrates as well as their spatial distribution patterns within the pores. The seismic velocities (P and S wave) showing an increasing trend with the increase in gas hydrate's saturation. Seismic velocities and densities effectively controls the seismic

reflectivity response, are the fundamental ingredients for AVO modeling and seismic attributes analysis.

In Fig. 2a–d, we have plotted the intercept, gradient, intercept versus gradient and their product, respectively for 11 samples at various gas hydrates saturations such as 0, 20, 30, 40 and 100 % by considering binary phase fluids (brine/gas hydrate). It has already been discussed that there is a gas layer present beneath the BSR, which results into strong negative impedance. Therefore, the intercept plot (Fig. 2a) shows strong negative values which gradually increase with increase in gas hydrates saturation. The gradient of gas hydrates present in the study area is also negative (Fig. 2b). However, gradient increases negatively as gas hydrates saturation increase. Since both intercept and gradient have negative values for different saturations (0, 20, 30, 40, 100 %) of gas hydrates, therefore in the intercept–gradient plots lies in the quadrant III (Fig. 2c). With the increase in gas hydrates saturation the deviation of gas hydrated sediments become more from the brine saturated sediments. $I * G$ is also fruitful indicator to discriminate gas hydrate reservoir and it shows positive behavior for gas hydrate bearing sediments and less positive for brine saturated sediments as shown in Fig. 2d.

In the Fig. 3a, b, we have also analyze $(I + G)/2$ and $(I - G)/2$ attributes to distinguish BSR. In the case of $(I + G)/2$ gas hydrate saturated sediments shows strongly negative deviation from brine saturated sediments (Fig. 3a), but in case of $(I - G)/2$ deviation for gas hydrate is negatively decreasing as compare to brine saturated sediments but deviation contrast is very small as shown in Fig. 3b. *PR* variation depends on Poisson ratio and it can be determined by converting seismic velocities in Poisson ratio. Mostly in gas hydrate/

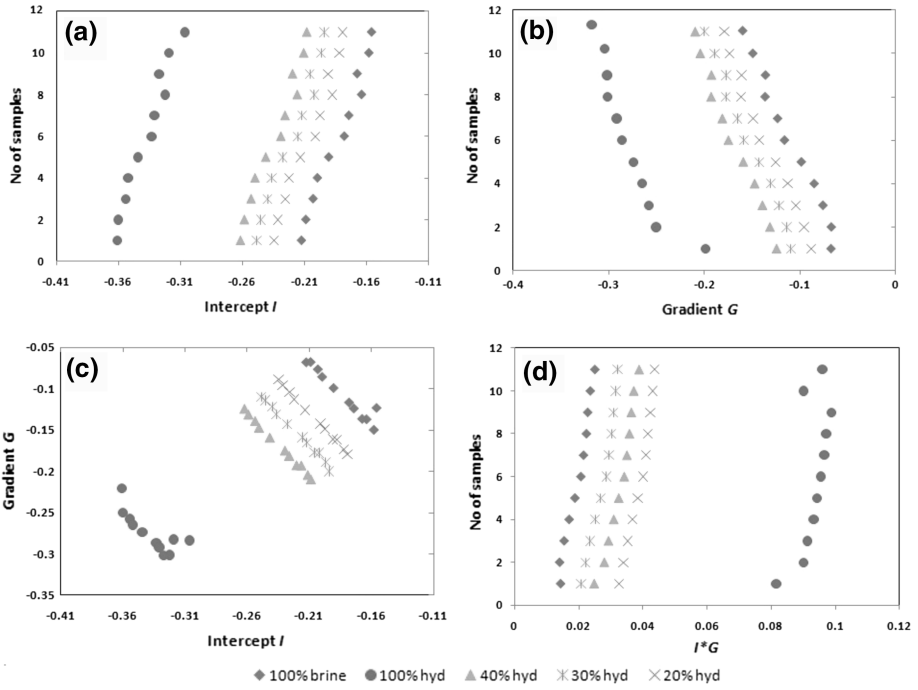

Fig. 2 **a** Intercept (I) response for different gas hydrate saturation (hyd), **b** gradient response for different gas hydrate saturation, **c** intercept versus gradient plot for different gas hydrate saturation, and **d** product of intercept (I) and gradient (G) for different gas hydrate saturations

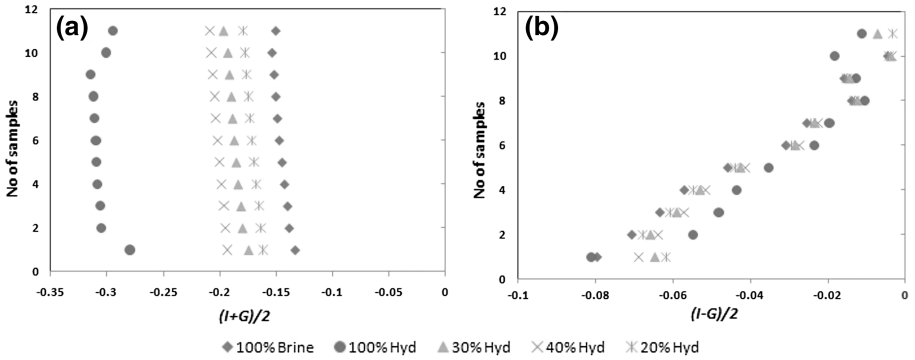

Fig. 3 **a** $(I + G)/2$ deviation trend for different gas hydrate saturation and **b** $(I - G)/2$ for different gas hydrate saturation

water layer, Poisson's ratio increases with increase of gas hydrate saturation. Because the gas hydrates layer have high P to S wave velocities ratio.

In gas layer Poisson's ratio is much lesser from gas hydrate layer. We have computed *PR* between gas hydrate layer and gas layer by considering 100, 40, 30, and 20 % gas hydrate saturation. In Fig. 4a *PR* contrast between gas hydrate-bearing sediments and brine saturated sediments helps to separate BSR easily. The reason of strong *PR* for gas hydrate layer is due to high difference in Poisson's ratio between gas hydrate layer and gas layer. In case of fully brine saturated sediments, Poisson's ratio contrast is not too much high so *PR* is not strongly negative if we will compare with gas hydrate saturated sediments as clearly shown in Fig. 4a. We have also plotted intercept versus *PR* in Fig. 4b which very clearly discriminate gas hydrate saturated sediments from brine saturated sediments along the both axis.

Fluid factor is an admirable attribute to determine gas hydrate bearing sediments. Usually fluid factor (ΔF) reflection shows near to 0 values when sediments are fully saturated with brine. When sediments are saturated with gas hydrate bearing sediments ΔF reflection shows negatively increasing trend from brine saturated sediments. In Fig. 5a the fluid factor for different gas hydrate saturation level is demonstrated. We have been clearly identify, when saturation of gas hydrate increase fluid factor reflections shows more negative deflection from 100 % brine saturated sediments. In Fig. 5b we have plotted fluid factor against intercept. A prominent separation has been identified between gas hydrate pay sand facies and water bearing sand facies.

K_P and $\lambda * \rho$ has been plotted in Fig. 6a, b with number of samples and our cross plot results reveals that pore space modulus and $\lambda * \rho$ also shows a reasonable deviation for gas hydrate bearing sediments.

4.1 Fluid indicator coefficients (FICs)

FIC has great tendency to compute the seismic attributes values broadly for accurate distinguishness between gas hydrates and water sediments. Highest value of FIC leads us towards a prominent discrimination between gas hydrate sediments and water saturated sediments. We have computed FIC deviation trend for different seismic attributes by taking gas hydrate saturation 100, 40, 30, 20 % (Fig. 7a–d), respectively. Our results reveal that FICs of ΔF, $I * G$, K_P, $\lambda * \rho$, *PR*, $(I + G)/2$ are higher (Fig. 7) than that of all other

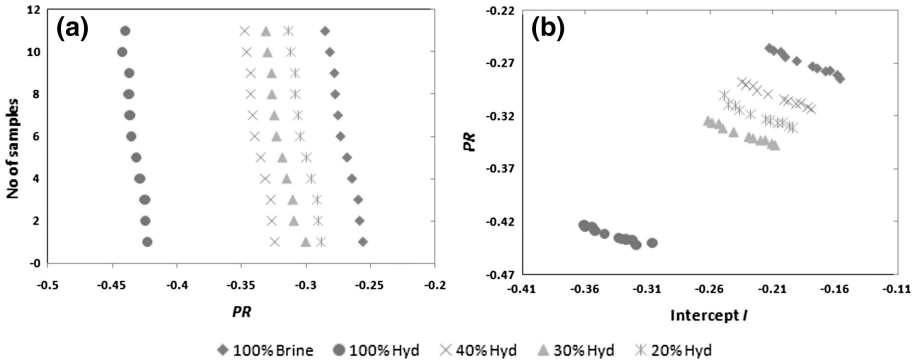

Fig. 4 **a** Poisson reflectivity (*PR*) versus number of samples for different gas hydrates saturation and **b** intercept (*I*) versus Poisson reflectivity response for different gas hydrate saturation

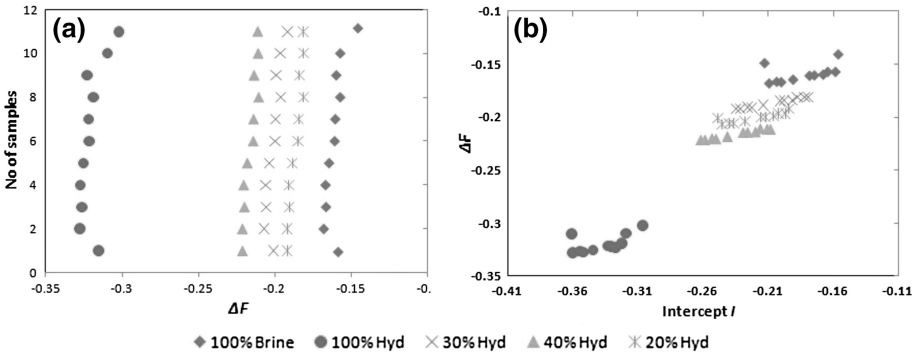

Fig. 5 **a** Fluid factor (ΔF) for different gas hydrate saturations and **b** fluid factor versus intercept deviation response for different gas hydrate saturation

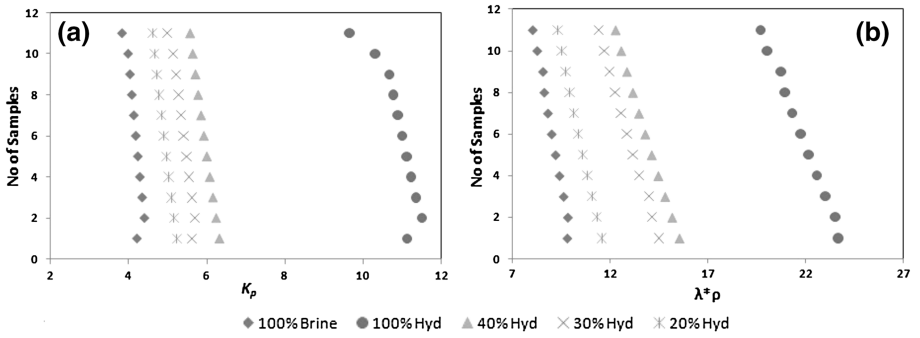

Fig. 6 **a** Pore space modulus (K_P) for various gas hydrate saturations and **b** $\lambda * \rho$ deviation response for different gas hydrate saturation

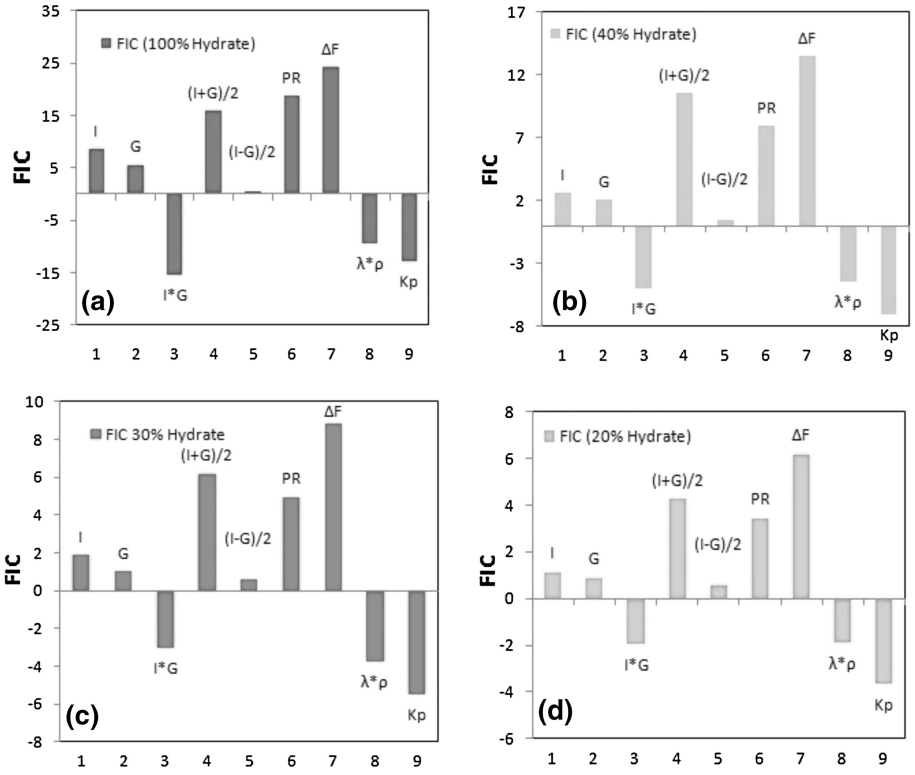

Fig. 7 **a** Fluid indicator coefficients at 100 % gas hydrates saturation for different attributes, **b** FIC deviation response for different attributes at 40 % gas hydrate saturation, **c** FIC at 30 % gas hydrate saturation and **d** FIC at 20 % gas hydrate saturation

attributes for different gas hydrate saturations indicating that these are more promising attributes that can be used to identify BSR. Derived values of FICs for each attributes are given in Table 2.

5 Conclusions

AVO analysis is performed on gas hydrate-bearing sediments and underlying free gas interval in Makran area of Pakistan, for quantitative assessment of gas hydrates saturation. Delicately, it is observed that intercept and gradient shows a negatively increasing trend for gas hydrate-bearing sediments. In gas hydrate reservoir sample to sample variation for intercept and gradient and all other attributes imprints different trends. Fluid factor, pore space modulus and *PR* shows negatively increasing trend. Critically analyzing behavior of different attributes shows that some attributes does not show clear deviation trend for gas hydrate bearing sediments from water sand. FIC demonstrates the authenticity of *PR*, ΔF, K_P, $I * G$, $(I + G/2)$ by showing a strong sensational trend for gas hydrate bearing sediments. Finally from our results, we have concluded that seismic attributes provide initiative basement for depiction of gas hydrate bearing sediments in Makran area of Pakistan.

Table 2 Fluid indicator coefficient values for different gas hydrate saturation

Attributes	*I*	G	I * G	(I + G)/2	(I − G)/2	*PR*	ΔF	λρ	K_P
Mean 100 %									
Brine	−0.18315	−0.1074	0.019669	−0.14288	−0.02036	−0.27076	−0.15907	9.001993	4.134962
Standard deviation	0.020734	0.029486	0.00388	0.014187	0.083333	0.009899	0.008214	0.611167	0.171719
Mean 100 %									
Gas hydrate	−0.33736	−0.27209	0.093162	−0.30472	−0.03264	−0.43278	−0.31942	21.75762	10.87449
Standard deviation	0.01817	0.029529	0.004779	0.009969	0.022398	0.006667	0.008544	1.351803	0.52529
FIC	8.487332	5.577052	−15.3784	15.96066	0.548259	18.76855	24.30177	−9.43601	−12.7955
Mean 40 %									
Gas hydrate	−0.23424	−0.1685	0.038932	−0.20137	−0.03287	−0.33681	−0.21619	13.8333	5.920703
Standard deviation	0.019677	0.03015	0.003857	0.005294	0.024901	0.008326	0.004247	1.086054	0.249087
FIC	2.596764	2.026457	−4.99468	10.53358	0.502551	7.933692	13.44961	−4.44849	−7.09614
Mean 30 %									
Gas hydrate	−0.22043	−0.14867	0.032993	−0.18637	−0.03679	−0.31953	−0.20057	12.90281	5.393216
Standard deviation	0.020017	0.040637	0.004363	0.006597	0.028781	0.009838	0.004718	1.041146	0.225382
FIC	1.862429	1.015506	−3.05379	6.178815	0.570842	4.95796	8.797121	−3.74666	−5.50209
Mean 20 %									
Gas hydrate	−0.2060	−0.1356	0.02736	−0.1709	−0.0352	−0.3017	−0.1863	10.3892	4.90880
Standard deviation	0.020346	0.032059	0.003961	0.005903	0.026192	0.009014	0.004413	0.748665	0.2065
FIC	1.126579	0.881109	−1.94161	4.27792	0.567003	3.439694	6.187337	−1.85297	−3.65936

Acknowledgments This research is related to PhD work of Mr. Muhammad Irfan Ehsan whose PhD is sponsored by China Scholarship Council. This work was done at the GeoSeis Modeling Lab of the Institute of Geology, University of the Punjab. The authors are thankful to the Institute of Geology for providing lab facilities.

References

Ahmed N, Khalid P, Ghazi S, Anwar AW (2015) AVO forward modeling and attributes analysis for fluid's identification a case study. Acta Geod Geophys. doi:10.1007/s40328-014-0097-x

Anderson AL, Bryant WR (1990) Gassy sediments occurance and properties northern Gulf of Mexico. Geo-Mar Lett 10:209–220

Andreassen K, Hart PE, Mary M (1997) Amplitude versus offset modeling of the bottom simulating reflection associated with submarine gas hydrates. Mar Geol 137:25–40

Burk C, Drake C (1974) The geology of continental margins. Springer, Berlin, pp 889–903

Carcione JM, Tinivella U (2000) Bottom-simulating reflectors: seismic velocities and AVO effects. Geophysics 65:54–67

Castagna JP, Backus M (1993) Offset dependent reflectivity: theory and practice of AVO analysis. Society of Exploration Geophysicists, Tulsa

Castagna JP, Smith SW (1994) Comparison of AVO indicators: a modeling study. Geophysics 59:1849–1855

Castagna JP, Swan HW, Foster DJ (1998) Framework for AVO gradient and intercept interpretation. Geophysics 63:948–956

Chen MP, Riedel M, Hyndman RD, Dosso SE (2007) AVO inversion of BSRs in marine gas hydrate studies. Geophysics 72:C31–C43

Dillon WP, Booth JS, Paul CK, Fehlhaber K, Hutchinson DR, Swift BA (1991) Mapping sub-seafloor reservoirs of a greenhouse gas: methane hydrate. In: International symposium on marine positioning, proceedings. Marine Technology Society, Washington, DC, pp 545–554

Dillon L, Schwedersky G, Asquez V, Velloso G, Nunes R (2003) A multi-scale DHI elastic attributes evaluation. Lead Edge 22:1024–1029

Ecker C, Dvorkin J, Nur A (1998) Sediments with gas hydrates: internal structure from seismic AVO. Geophysics 63:1659–1669

Ehsan IM, Ahmed N, Khalid P, Liu XW, Naeem M (2015) An application of rock physics modeling to quantify the seismic response of gas hydrate-bearing sediments in Makran accretionary prism, offshore, Pakistan. Geosci J. doi:10.1007/s12303-015-0044-z

Farhoudi G, Karig DE (1977) Makran of Iran and Pakistan as an active arc system. Geology 5:664–668

Gassmann F (1951) Über die Elastizität poröser Medien. Vierteljahrsschr Natforsch Ges Zür 96:1–23

Hardage BA, Roberts HH (2006) Gas hydrate in the Gulf of Mexico: what and where is the seismic target. Lead Edge 25:566–571

Harms JC, Cappel HN, Francis DC (1982) Geology and petroleum potential of the Makran Coast, Pakistan. In: 82th Offshore South East Asia conference, Singapore, 9–12 February. Society of Petroleum Engineers, pp 3–26

Hedlin K (2000) Pore space modulus and extraction using AVO. In: 70th Annual international meeting, SEG expanded abstracts, pp 170–173

Hill R (1963) Elastic properties of reinforced solids: some theoretical principles. J Mech Phys Solids 11:357–372

Hyndman RD, Spence GD (1992) A seismic study of methane hydrate marine bottom simulating reflectors. J Geophys Res 97:6683–6698

Khalid P, Broseta D, Nichita DV, Blanco J (2014) A modified rock physics model for analysis of seismic signatures of low gas-saturated rocks. Arab J Geosci 7:3281–3295. doi:10.1007/s12517-013-1024-0

Kvenvolden KA (1998) A primer on the geological occurrence of gas hydrate. In: Henriet JP, Mienert J (eds) Gas hydrates: relevance to the world margin stability and climate change. Special publications, vol 137. Geological Society, London, pp 9–30

Makogon YF, Holditch SA, Makogon TY (2007) Natural gas hydrate a potential energy source for the 21st century. J Pet Sci Eng 56:14–31

Ojha M, Sain K (2008) Appraisal of gas hydrate/free-gas from VP/VS ratio in the Makran accretionary prism. Mar Pet Geol 25:637–644

Ojha M, Sain K (2009) Seismic attributes for identifying gas hydrates and free-gas zones: application to the Makran accretionary prism. Episodes 32:264–270

Ojha M, Sain K, Minshull AT (2010) Assessment of gas hydrates saturation in the Makran accretionary prism using offset dependence of seismic amplitudes. Geophysics 75:C1–C6
Paull CK, Ussler W, Dillon WP (1991) Is the extent of glaciation limited by marine gas-hydrates. Geophys Res Lett 18:432–434
Quittmeyer RC, Farah A, Jacob KG (1979) The seismicity of Pakistan and its relation to surface faulting. In: Farah A, DeJong KA (eds) Geodynamics of Pakistan. Geological Survey of Pakistan, Quetta, pp 45–67
Russell B, Hedlin K, Hilterman F, Lines L (2003) Fluid-property discrimination with AVO: a Biot–Gassmann perspective. Geophysics 68:29–39
Sain K, Gupta HK (2012) Gas hydrates in India: potential and development. Gond Res. doi:10.1016/j.gr.2012
Shuey RT (1985) A simplification of the Zoeppritz equations. Geophysics 50:609–614
Sloan ED (1998) Clathrate hydrate of natural gases. Marcel Dekker, Inc., New York
Smith GC, Gidlow PM (1987) Weighted stacking for rock property estimation and detection of gas. Geophys Prospect 35:993–1014
Stoneley R (1974) Evolution of the continental margins bounding a former southern Tethys. In: Sain K and Gupta HK (2012) Gas hydrates in India: potential and development. Gondwana Res 22:645–657
Taylor CE, Kwan JT (2004) Advances in the study of gas hydrates. Kluwer Academic/Plenum Publishers, New York
Verm R, Hilterman FJ (1995) Lithology color-coded seismic sections: the calibration of AVO crossplotting to rock properties. Lead Edge 14:847–853
White RS (1979) Deformation of Makran Continental margin. In: Farah A, De-Jong KA (eds) Geodynamics of Pakistan. Geological Survey of Pakistan, Quetta, pp 132–145
Yang R, Yan P, Wu N, Sha Z, Liang J (2014) Application of AVO analysis to gas hydrates identification in the northern slope of the South China Sea. Acta Geophys 62:810–817
Yuan T, Spence GD, Hyndman RD, Minshull TA, Singh SC (1999) Seismic velocity studies of a gas hydrate bottom-simulating reflector on the northern Cascadia continental margin, amplitude modeling and full waveform inversion. J Geophys Res 104:1179–1191
Zoeppritz K (1919) Erdbebenwellen VIIIB, on the reflection and propagation of seismic waves. Gott Nachr I:66–84